BIOCHEMISTRY
including biophysical chemistry & molecular biology

Article

pubs.acs.org/biochemistry

Dissecting Cytochrome P450 3A4–Ligand Interactions Using Ritonavir Analogues

Irina F. Sevrioukova[†,*] and Thomas L. Poulos[†,‡,§]

[†]Departments of Molecular Biology and Biochemistry, [‡]Chemistry, and [§]Pharmaceutical Sciences, University of California, Irvine, California 92697, United States

Supporting Information

ABSTRACT: Cytochrome P450 3A4 (CYP3A4) inhibitors ritonavir and cobicistat, currently administered to HIV patients as pharmacoenhancers, were designed on the basis of the chemical structure/activity relationships rather than the CYP3A4 crystal structure. To better understand the structural basis for CYP3A4 inhibition and the ligand binding process, we investigated five desoxyritonavir analogues to elucidate how substitution/elimination of the phenyl side groups (Phe-1 and Phe-2) and removal of the isopropyl-thiazole (IPT) moiety affect affinity, inhibitory potency, and the ligand binding mode. Our experimental and structural data indicate that the side group size reduction not only drastically lowers affinity and inhibitory potency for CYP3A4 but also leads to multiple binding modes. Regardless of the side group chemical nature and the number of molecules bound, the space adjacent to the 369–371 peptide and Arg105 (Phe-2 site) is always occupied and, hence, must be a critically important binding site. When possible, the ligands also try to fill the pocket near the I-helix (Phe-1 site), even if it causes steric hindrance. Extensive hydrophobic interactions established at the Phe-1 site improve inhibitory potency, whereas contacts provided by IPT might strengthen the Fe–N bond. Overall, however, the end group contributes less to the ligand association process, which, in contrast, is greatly facilitated by the polar interactions mediated by the active site Ser119.

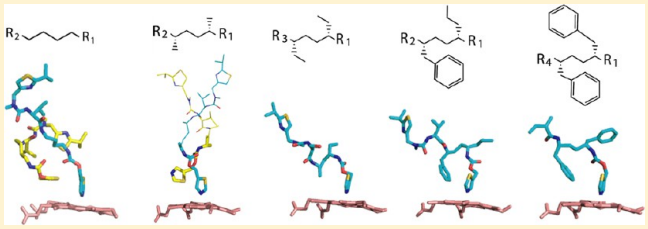

Human drug-metabolizing cytochrome P450 3A4 (CYP3A4) clears the majority of administered drugs through oxidative metabolism. Some drugs and metabolites can inactivate CYP3A4, leading to elevated plasma levels of pharmaceuticals and toxins. Controlled CYP3A4 inhibition, however, can be clinically beneficial. In HIV-infected patients, for instance, potent CYP3A4 inactivators ritonavir and cobicistat are administered to "boost" plasma levels of HIV protease inhibitors, which otherwise are quickly metabolized by CYP3A4. Ritonavir was originally designed as an HIV protease inhibitor [1] but was later found to act as a very potent inactivator of the CYP3A family of enzymes.[2] This peptidomimetic drug contains a thiazole headgroup, a midportion with two phenyl (Phe-1 and Phe-2) and one valine side groups, and the isopropyl-thiazole (IPT) end moiety (Figure 1A). Cobicistat is a ritonavir derivative that lacks the backbone hydroxyl group, resulting in the loss of the undesired anti-HIV protease activity, and has a morpholine ring instead of the valine side chain.[3,4] Both drugs were designed on the basis of structure/activity relationships rather than the CYP3A4 crystal structure, and therefore, the structural basis for their inhibitory mechanism is not fully understood.

To obtain mechanistic insights into inhibitor action, we previously investigated the CYP3A4 interaction with ritonavir and two analogues, deazaritonavir and desthiazolylmethyl-oxycarbonyl ritonavir (DTMCR, Figure 1A), lacking the heme-ligating thiazole nitrogen or the entire thiazole head-group, respectively.[5,6] These studies suggested that heme ligation is essential for tight association of ritonavir and that the strong and irreversible binding rather than formation of reactive metabolites is the key contribution to CYP3A4 inhibition. Unable to ligate to the heme iron, deazaritonavir acts as a type I ligand, causing a partial low-to-high spin shift, and dissociates from CYP3A4 during crystallization.[6] DTMCR, on the other hand, ligates *via* the amino group reversibly and with a 70-fold lower affinity, but its inhibitory potency is only 4-fold lower than that of ritonavir. One explanation for this phenomenon was provided by the X-ray structure of the CYP3A4–DTMCR complex,[6] showing that DTMCR rotates by 180° to place the phenyls into hydrophobic pockets similarly to ritonavir (Figure 1B). This led us to suggest that nonbonding interactions provided by the side groups are important and determine the binding orientation.

In a subsequent study, we investigated how CYP3A4 interacts with three derivatives of desoxyritonavir (the back-bone present in cobicistat) where the heme-ligating thiazole was substituted with the imidazole, oxazole, or pyridine groups (designated here as GS1, GS2, and GS3, respectively).[7] GS1 binds to CYP3A4 with high affinity but reversibly and, like deazaritonavir, dissociates during crystallization. The high inactivation potency of GS1 was due to its ability to cause a

Received: April 30, 2013
Revised: June 2, 2013
Published: June 7, 2013

   dx.doi.org/10.1021/bi4005396 | *Biochemistry* 2013, 52, 4474–4481

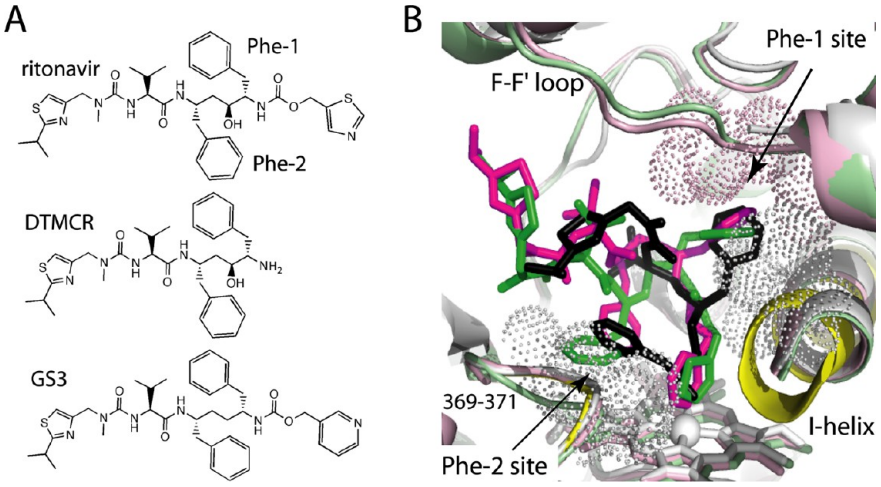

Figure 1. Chemical structures (A) and the binding mode (B) of ritonavir, DTMCR, and GS3 in the CYP3A4 active site. Ritonavir and the corresponding structure are shown in green, the DTMCR-bound structure in black and white, and the CYP3A4–GS3 complex in magenta and pink (PDB ID codes 3NXU, 3TGS, and 4I4H, respectively). For comparison, the I-helix and the 369–371 peptide of the ligand-free CYP3A4 (1TQN structure) are displayed in yellow. The I-helix shifts upon binding of all three ligands, whereas the 369–371 peptide is distorted only in the ritonavir-bound CYP3A4. The Phe-1 and Phe-2 binding sites are indicated. To optimize hydrophobic interactions *via* the side groups, DTMCR rotates by 180° relative to ritonavir.

large decrease in the heme redox potential, which precludes electron transfer. GS2 is a lower affinity ligand and a less potent CYP3A4 inhibitor that remains bound to the active site during crystallization. However, only the heme-ligating oxazole was defined in the X-ray structure, while the rest of GS2 was disordered. In contrast, GS3 (Figure 1A) was found to be a stronger ligand and a more potent CYP3A4 inhibitor than ritonavir, and all but the IPT part of GS3 were observed in the crystal structure.[7] Owing to more favorable stereoelectronic properties of the pyridine nitrogen and a more flexible backbone, GS3 ligates to the heme iron tighter and forms a stronger H-bond with Ser119, a key active site residue regulating the protein–ligand association. Another advantage is that the GS3 binding mode eliminates steric clashing through Phe-2 and promotes cation–π and π–π interactions that cannot be established by ritonavir. One unfavorable interaction, however, a clash between Phe-1 (Phe-2 in DTMCR) and Phe304 leading to the I-helix displacement, remains in the GS3-bound CYP3A4 (Figure 1B).

To gain further insights into the mechanism of CYP3A4 inhibition and ligand binding, we tested how Phe-1/Phe-2 substitution and IPT removal affect affinity, inhibitory potency, and the ligand binding mode using compounds GS4, GS5, and GS6, where both phenyl groups were eliminated or substituted with the methyl or ethyl groups, respectively, with one additional change in GS6 (a valine-to-serine side chain substitution); GS7, containing the propyl chain instead of Phe-1; and GS8, containing both phenyl groups but lacking IPT (Figure 2). The results presented here provide further evidence for the high flexibility and adaptability of the CYP3A4 active site and its ability to accommodate multiple ligands, and show that the binding mode, affinity, and inhibitory potency of desoxyritonavir analogues are greatly affected by the chemical nature of the side groups and Ser119-mediated polar interactions, with IPT playing a less important role.

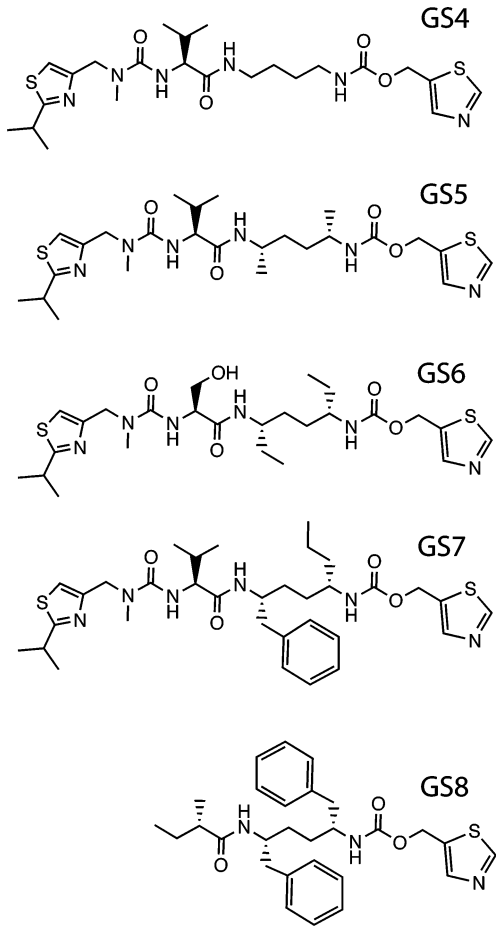

Figure 2. Chemical structures of GS4–GS8.

MATERIALS AND METHODS

Protein Expression and Purification. C-terminal 4-histidine tagged wild type (WT) CYP3A4Δ3-22 and the S119A mutant were produced, purified, and quantified as reported previously.[5]

Spectral Binding Titrations. Ligand binding to CYP3A4 was monitored in 50 mM phosphate, pH 7.4, containing 20% glycerol and 1 mM dithiothreitol (buffer A) in a Cary 3

dx.doi.org/10.1021/bi4005396 | *Biochemistry* 2013, 52, 4474–4481

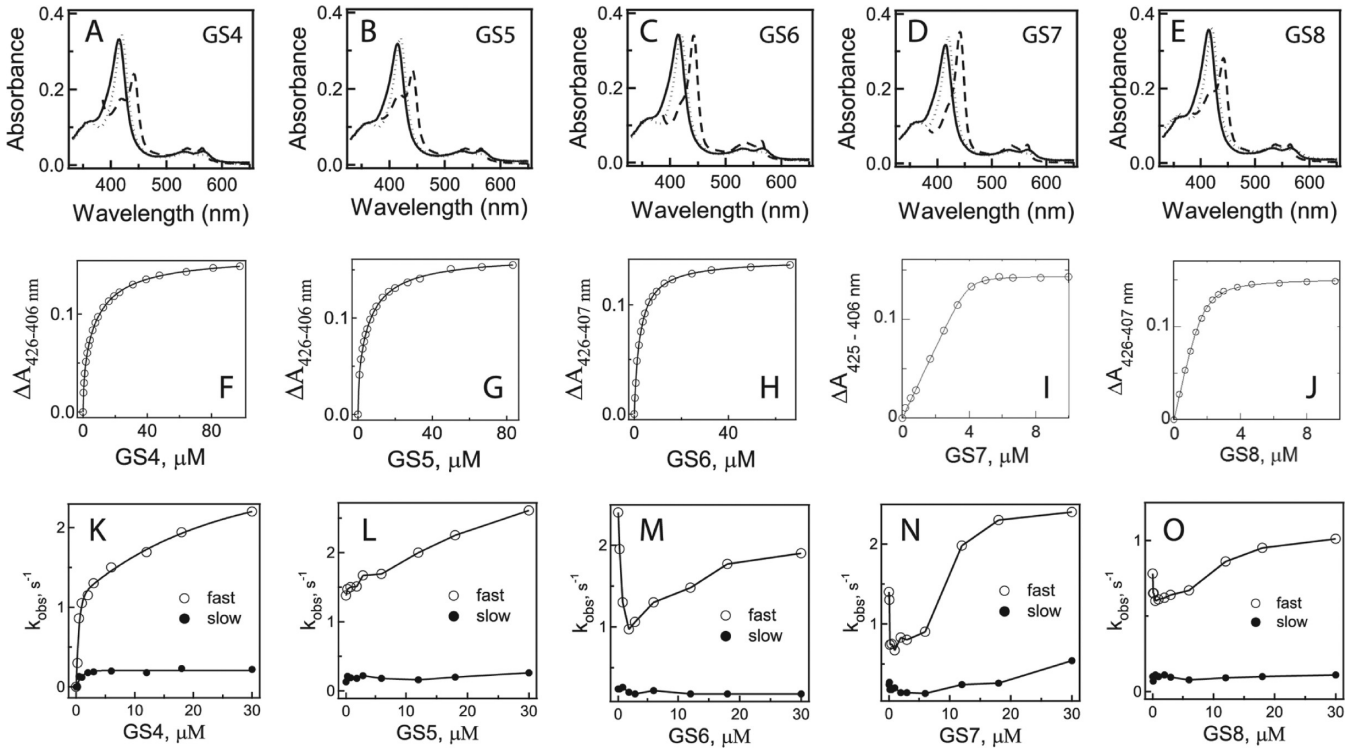

Figure 3. (A–E) Absorbance spectra of ligand-free (—) and the ferric (···) and ferrous (- - -) forms of the GS4–GS8-bound CYP3A4. (F–J) Titration plots for GS4–GS8. (K–O) Plots of the rate constants for the fast (○) and slow phases (●) of the GS4–GS8 binding reaction vs ligand concentration. The estimated K_s and limiting k_{fast} values are given in Table 1.

spectrophotometer. The protein was titrated with small aliquots of dimethyl sulfoxide (DMSO) solutions of GS4, GS5, GS6, GS7, or GS8 (Gilead Sciences), with the final solvent concentration <2%. Spectral dissociation constants (K_s) were determined from the titration curves.

Kinetics of Ligand Binding. The kinetics of ligand binding to CYP3A4 was monitored at room temperature in 50 mM phosphate, pH 7.4, in a SX.18MV stopped flow apparatus (Applied Photophysics, U.K.). After mixing 2 μM protein solutions with various concentrations of ligands, absorbance changes were followed at 425–426 nm. Kinetic data were analyzed using the IgorPro program (WaveMetrics, Inc.).

Thermal Denaturation and Inhibitory Potency Assays. Thermal denaturation experiments were conducted to compare ligand-dependent changes in CYP3A4 stability as previously described.[7] The denaturation midpoint (melting temperature, T_m) was determined as the temperature at which both the folded and unfolded states are equally populated. The inhibitory potency of GS4–GS8 on the 7-benzyloxy-4-(trifluoromethyl)coumarin hydroxylase activity of CYP3A4 was evaluated fluorometrically in a reconstituted system with rat cytochrome P450 reductase according to a previously reported procedure.[7] The concentration required for half-maximal inactivation (IC_{50}) was derived from the [% activity] vs [inhibitor] plots.

Crystallization and Determination of Ligand-Bound CYP3A4 Crystal Structures. CYP3A4 was cocrystallized with GS4–GS8 by a microbatch method under oil. CYP3A4 (50–55 mg/mL) in buffer A was mixed with ligands (5–10-fold excess) and centrifuged to remove the precipitate. A half microliter of ligand-bound CYP3A4 was mixed with 0.5 μL of 10–12% polyethylene glycol 3350 and 90–100 mM sodium malonate, pH 5.0–6.0, and covered with paraffin oil. Crystals were harvested a few days later and frozen in liquid nitrogen using Paratone-N oil as a cryoprotectant. X-ray diffraction data were collected at the Stanford Synchrotron Radiation Lightsource beamline 7-1 and the Advanced Light Source beamline 8.2.1. Crystal structures were solved by molecular replacement with PHASER[8] and the 3NXU structure as a search model. The initial models were rebuilt and refined with COOT [9] and REFMAC.[8] Data collection and refinement statistics are summarized in Supporting Information Table 1S. The atomic coordinates and structure factors for GS4-, GS5-, GS6-, GS7-, and GS8-bound CYP3A4 have been deposited to the Protein Data Bank with the ID codes 4K9T, 4K9U, 4K9V, 4K9W, and 4K9X, respectively.

RESULTS

Decrease in Size and Elimination of the Desoxyritonavir Side Groups Lower Affinity for CYP3A4 and Lead to Multiple Ligand Binding Modes. Association of GS4–GS8 with CYP3A4 was accompanied by a red shift in the Soret band (415 to 420–421 nm), indicative of type II ligand binding *via* formation of the Fe–N bond. The 442 nm absorption of the ferrous species, thought to reflect the Fe–N bond strength,[7] depended on the ligand chemical structure and increased in the following order: GS4 > GS5 > GS8 > GS6 > GS7 (Figure 3A–E). Spectral dissociation constants (K_s) calculated from the titration plots (Figure 3F–J) indicate that GS7 has the highest affinity for CYP3A4, comparable to that of ritonavir and GS3 (40 nM vs 50 and 25 nM, respectively). The K_s values for GS8 and GS6 are 4- and 58-fold lower, respectively, whereas the titration plots for GS4 and GS5 are consistent with the two-site binding and two affinities differing by 8–18-fold (Table 1).

The kinetics of GS4–GS8 ligation are biphasic, with the rate constants for the fast phase (k_{fast}) weakly affected by the side

dx.doi.org/10.1021/bi4005396 | *Biochemistry* 2013, 52, 4474–4481

Table 1. Properties of the Desoxyritonavir Analogues

	K_s[a] (μM)	k_{fast}[b] (s^{-1})	ΔT_m[c] (°C)	IC_{50}[d] (μM)
GS3	0.025 ± 0.005[e]	7.0 ± 0.5[e]	6.7 ± 0.3[e]	0.13 ± 0.02[e]
GS4	1.5 ± 0.2	2.1 ± 0.3	1.1 ± 0.2	15.0 ± 1.0
	13.1 ± 1.0			
GS5	0.4 ± 0.1	2.6 ± 0.3	1.3 ± 0.1	10.0 ± 1.0
	7.3 ± 0.5			
GS6	2.3 ± 0.1	1.9 ± 0.2	1.7 ± 0.2	9.7 ± 0.7
GS7	0.04 ± 0.01	2.4 ± 0.3	3.5 ± 0.2	2.8 ± 0.3
GS8	0.16 ± 0.01	1.0 ± 0.1	4.1 ± 0.2	1.3 ± 0.3

[a]Spectral dissociation constant. [b]Rate constant for the fast phase of the binding reaction measured at 30 μM ligand concentration. [c]Changes in the melting temperature of CYP3A4 caused by ligand binding. T_m for ligand-free CYP3A4 in the presence of 2% DMSO is 52.1 ± 0.1 °C. [d]Concentration required for half-maximal inactivation of recombinant CYP3A4. [e]Determined previously.[7]

chain modifications or IPT removal (Table 1). However, the k_{fast} vs [ligand] plot is hyperbolic only for GS4 and atypical (near linear or V-shaped) for other compounds (Figure 3K–O). Thus, the side groups of ritonavir-like molecules not only affect the binding affinity but also complicate the heme ligation kinetics.

Effect of Structural Variations on Inhibitory Potency and Thermal Stability of Ligand-Bound CYP3A4. Previously we reported that thermal denaturation can serve as an additional tool for evaluating ligand-induced changes in CYP3A4 because the melting temperature (T_m) shifts correlate with ligand affinity.[7] All investigated compounds increased the thermal stability of CYP3A4, with the largest ΔT_m observed upon GS8 and GS7 binding (4.1 and 3.5°, respectively; Table 1). Accordingly, our CYP3A4 inhibition assays showed that GS7 and GS8 had the lowest IC_{50} (2.8 and 1.3 μM, respectively), which for other compounds was within the 9–15 μM range (Table 1). This implies that extensive hydrophobic interactions provided by the phenyl side groups increase the inhibitory potency and stabilize the ligand-bound CYP3A4.

Effect of the Ser119Ala Mutation on CYP3A4 Interaction with GS4–GS8. The active site residue Ser119 assists formation and increases stability of the CYP3A4 complexes with ritonavir and GS3, in part, through H-bonding with the ligand backbone atoms.[7] To test whether Ser119 plays any role in association of GS4-GS8, we analyzed how the S119A mutation affects affinity and binding kinetics. It was found that the S119A replacement (i) decreases the 442 nm absorption of the ferrous ligand-bound CYP3A4, most notably for the GS4- and GS5-bound species, (ii) eliminates the second binding site for GS4 and GS5, (iii) lowers K_s for GS4 and GS5 by 2 orders of magnitude and for GS6-GS8 by 3–14-fold, and (iv) perturbs the GS4–GS8 heme binding kinetics (Figure 4, Table 2, Supporting Information Figure 1S). The reactions of GS4, GS5, and GS8 ligation to CYP3A4 S119A became monophasic and proceeded 3–5-fold more slowly. Although the binding process for GS7 and GS8 remained biphasic, the k_{fast} values were decreased by 10–20-fold relative to those for WT (Tables 1 and 2). The S119A mutation also affected the stability of the GS4-GS8-bound protein. T_m shifts induced by GS7 and GS8 were smaller (1.1–1.6° vs 3.5–4.1° for WT), whereas the stabilizing effect of GS4, GS5 and GS6 was completely abolished (Table 2). Thus, Ser119 markedly

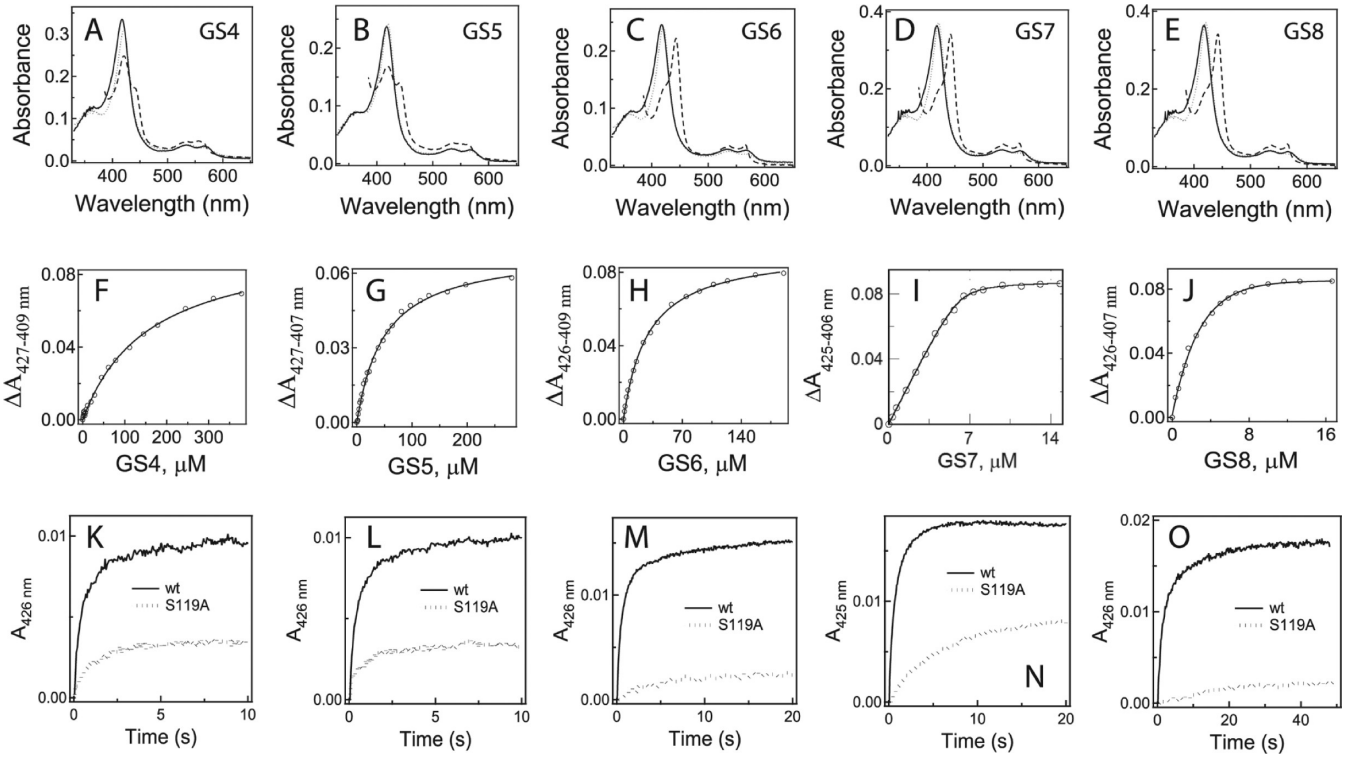

Figure 4. Effect of the S119A mutation on the GS4–GS8 affinity and binding kinetics. (A–E) Absorbance spectra of ligand-free (—) and the ferric (···) and ferrous (- - -) forms of the GS4-GS8-bound CYP3A4 S119A. (F–J) Titration plots for GS4–GS8. (K–O) Kinetics of GS4–GS8 binding to the heme of WT and S119A CYP3A4 (solid and dotted traces, respectively) recorded at 30 μM ligand concentration. The estimated K_s and limiting k_{fast} values are given in Table 2.

dx.doi.org/10.1021/bi4005396 | Biochemistry 2013, 52, 4474–4481

Table 2. Effect of the S119A Mutation on the CYP3A4 Interaction with GS4-GS8

	K_s (μM)	k_{fast} (s^{-1})	ΔT_m (°C)[a]
GS4	160 ± 10	0.70 ± 0.10[b]	−0.2 ± 0.1
GS5	50 ± 3	0.72 ± 0.09[b]	0
GS6	33 ± 4	0.35 ± 0.03	0.2 ± 0.1
GS7	0.14 ± 0.03	0.24 ± 0.02	1.6 ± 0.2
GS8	1.4 ± 0.2	0.05 ± 0.01[b]	1.1 ± 0.2

[a]Changes in the melting temperature of CYP3A4 S119A caused by ligand binding. T_m for the ligand-free S119A mutant in the presence of 2% DMSO is 53.5 ± 0.1 °C. [b]Reactions of CYP3A4 S119A binding to GS4, GS5, and GS8 were monophasic.

facilitates association of GS4−GS8 and stabilizes the resulting complexes.

Crystal Structures of GS4−GS8-Bound CYP3A4. Despite widely different binding affinities, all compounds willingly cocrystallized with CYP3A4, allowing us to solve the X-ray structures to 2.40−2.85 Å resolution (Supporting Information Table 1S). Since GS3 is the most potent CYP3A4 inhibitor[7] and, similar to GS4-GS8, has the desoxyritonavir backbone (Figure 1A), the CYP3A4−GS3 complex structure (PDB ID 4I4H) was used for comparative analysis.

CYP3A4−GS8 Complex. GS8 contains both phenyl side groups but lacks IPT (Figure 2). In the crystal structure, only the GS8 thiazole and phenyl side groups are clearly defined (Figure 5A). The truncated tail portion can be traced when an electron density map is contoured at a lower σ level (Supporting Information Figure 3S). GS8 is positioned similarly to GS3 and forms near identical contacts *via* Phe-1 and Phe-2. Phe304 and the I-helix are displaced to the same extent because of steric hindrance with Phe-1 (Figure 5B,C). The main differences are a longer distance between the GS8 carbonyl oxygen and Ser119:OH (3.5 vs 2.5 Å in GS3; Figure 5D) and a disordered F−F′ loop (residues 211−217), which leaves the active site open to solvent (Supporting Information Figure 4S).

CYP3A4−GS7 Complex. GS7 has the propyl group instead of Phe-1 (Figure 2) but maintains high affinity for CYP3A4. The CYP3A4-GS7 complex crystallizes in space group *P*3, with

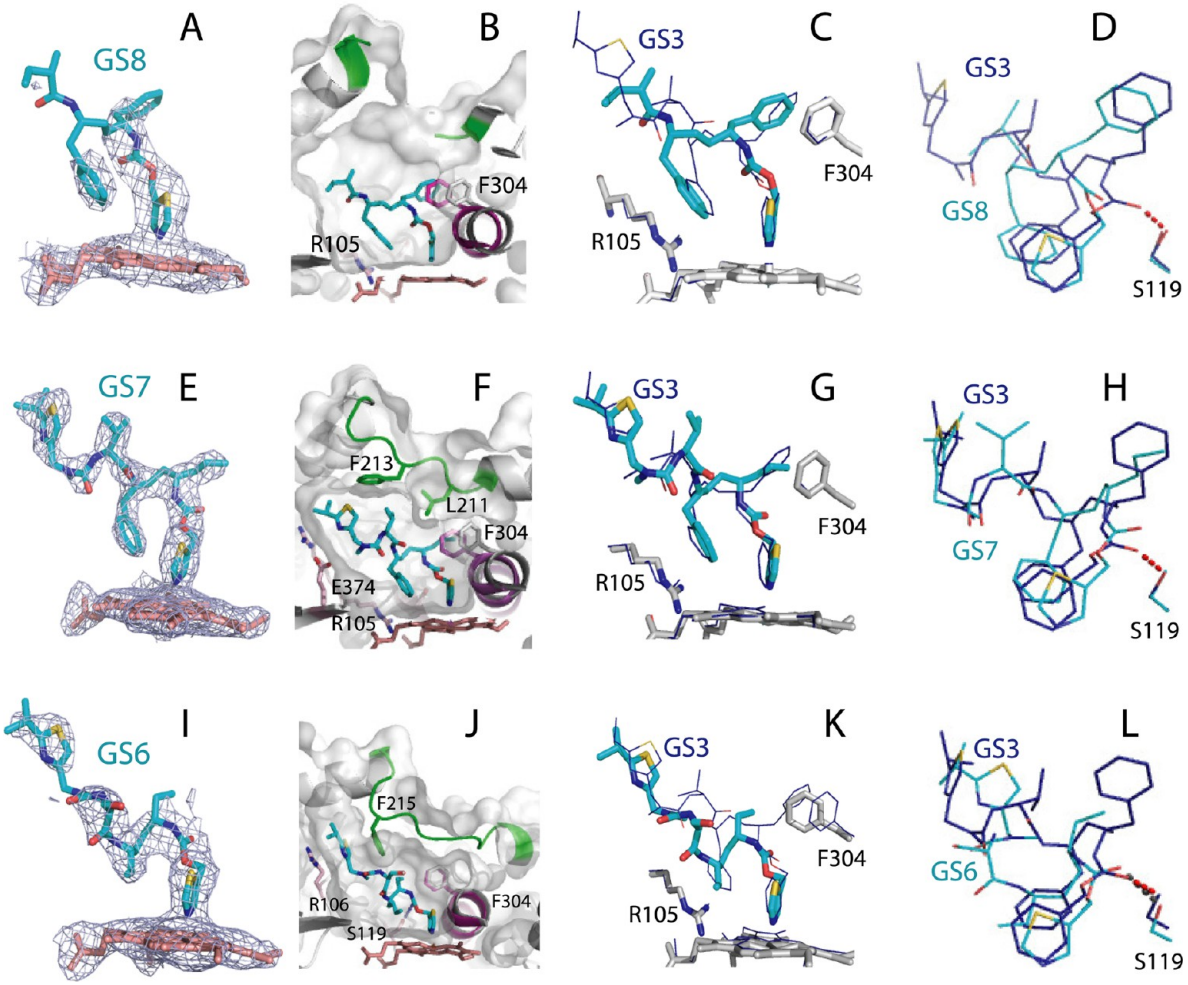

Figure 5. Crystal structures of the GS8- (A−D), GS7- (E−H), and GS6-bound (I−L) CYP3A4. Panels A, E, and I show $2F_o - F_c$ electron density maps at the heme and ligands contoured at 1σ. Panels B, F, and J demonstrate how ligands are positioned in the active site. The side chains of selected residues are in stick representation, and the F−F′ loop is in green. For comparison, the I-helix and Phe304 of ligand-free CYP3A4 are displayed in magenta. Panels C, D, G, H, K, and L show a superimposed GS3-bound structure (in dark blue and line representation) to emphasize differences in the ligand binding mode. Panels D, H, and L give a closer view at the Ser119 site. Only GS3 and GS6 can form a hydrogen bond with Ser119 (depicted as red and black dotted lines, respectively).

dx.doi.org/10.1021/bi4005396 | *Biochemistry* 2013, 52, 4474−4481

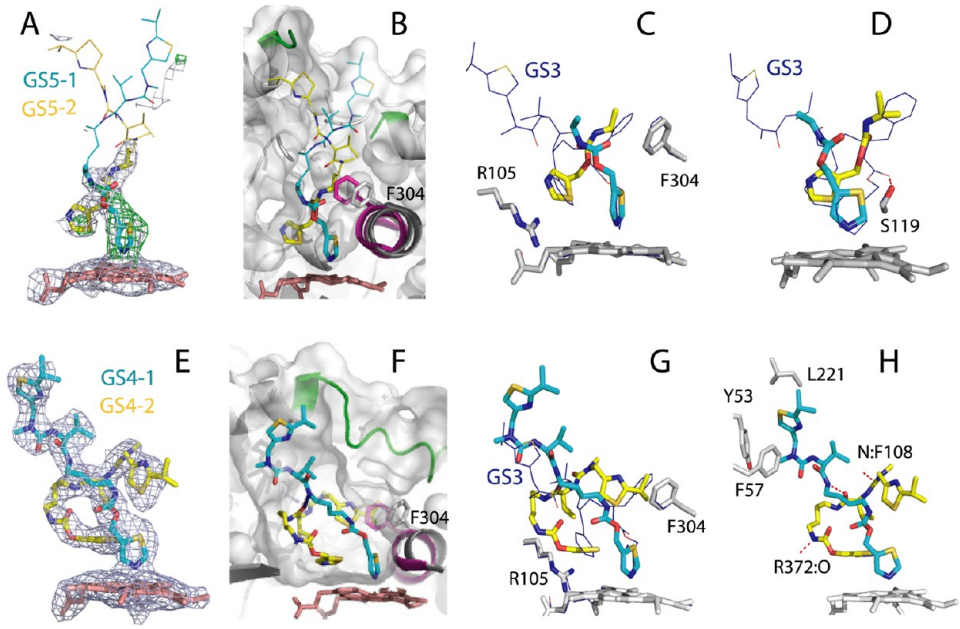

Figure 6. Crystal structures of the GS5- (A–D) and GS4-bound (E–H) CYP3A4. In both structures, there are two ligands present in the active site, colored in cyan and yellow. The parts of GS5-1 and GS5-2 defined in the X-ray structure are in a stick representation, whereas the arbitrarily modeled disordered parts are shown as thin lines. Panels A and E show $2F_o - F_c$ electron density maps at the heme and ligands contoured at 1σ. Panels B and F show the active site cavity, where the I-helix and Phe304 of ligand-free CYP3A4 are displayed in magenta. The F–F′ loop (in green) is disordered in the GS5-bound structure. Panels C, D, and G provide different views at the superimposed GS3-bound structure (in dark blue and line representation) to highlight differences in the ligand binding mode. Panels C and D display only portions of GS5-1 and GS-2 that are visible in the crystal structure. In panel H, hydrogen bonds formed by the GS4-2 molecule are depicted as red dotted lines.

four molecules per asymmetric unit. The ligand is similarly oriented in all four molecules but is better defined in molecule C, which will be described here. The electron density for GS7 was continuous (Figure 5E) and allowed unambiguous fitting. GS7 also adopts a GS3-like conformation (Figure 5E–G), with the propyl chain occupying the Phe-1 site and displacing Phe304 and the I-helix to the same extent. The latter finding was quite surprising considering a smaller size and higher flexibility of the propyl group. Most notable dissimilarities with the GS3-bound structure are (i) a shifted GS7 thiazole plane (~30° rotation), (ii) no H-bonding to Ser119 (distance between GS7:O and Ser119:OH is 3.4 Å), and (iii) a different orientation of the GS7 valine chain, which leads to the F–F′ loop rearrangement and more optimal hydrophobic interactions with Leu211 and Phe213. The thiazole ring rotation and loss of the H-bond to Ser119 are the result of stretching in the thiazole-connecting linker, without which the propyl group cannot be placed at the Phe-1 site (Figure 5H).

Similar to ritonavir, the GS7 IPT nitrogen is directed toward a cluster of charged residues (in particular, Arg106 and Glu374) and positioned suitably for polar interactions. Owing to a differently folded F–F′ loop, the IPT sulfur is closer to the Phe213 ring and, unlike the ritonavir end group, can form S–π interactions (Figure 5F and Supporting Information Figure 2S). Since the GS3 tail is not seen in the crystal structure and was modeled based on the ritonavir orientation,[7] it is unclear whether GS3 establishes similar contacts. Nevertheless, the fact that GS7 inactivates CYP3A4 less potently than GS8, GS3, and ritonavir (IC_{50} of 2.8 μM vs 1.3 μM, 130 nM, and 550 nM, respectively) suggests that Phe-1 is one of the elements that impart inhibitory potency.

CYP3A4–GS6 Complex. Having a serine- and two ethyl-substituted side chains (Figure 2), GS6 adopts a distinct conformation in the CYP3A4 active site. Mostly continuous electron density (Figure 5I) is indicative of a deeper curvature in the backbone, which enables GS6 to fill the Phe-2 site with its ethyl and main chain atoms (Figure 5I–K). The Phe-1 site remains unoccupied, and hence, there is no I-helix shift. Owing to the higher polarity of the serine side group, the GS6 midportion moves toward and forms polar contacts with the carbonyl oxygens of residues 369, 370, 372, and 481. Consequently, the F–F′ loop adopts a new conformation in order to optimize interactions with the tail portion of GS6. IPT is now sandwiched between the parallel Phe215 ring and the Arg106 guanidinium group (Figure 5J), thereby promoting π–π and cation–π interactions. These newly established interactions, as well as the H-bonding to Ser119 and complete sequestration from the solvent (Figure 5L and Supporting Information Figure 4S), could partially compensate for the loss of the Phe-1/Phe-2-mediated contacts.

CYP3A4–GS5 Complex. GS5 has two methyl side groups instead of phenyls (Figure 2) and, according to the spectral data, has two binding sites in CYP3A4. The electron density present in the active site indicates that, indeed, there are two intertwined molecules (GS5-1 and GS5-2) bound in an extended conformation, whose tails are not seen due to structural disorder (Figure 6A–C). Notably, heme-ligating GS5-1 rotates by 180° relative to GS3 (compare thiazole orientations in Figure 6D) to allow GS5-2 to bind along and occupy both hydrophobic pockets. The GS5-2 thiazole is at the Phe-2 site, sandwiched between the GS5-1 thiazole and Arg105 guanidinium groups, whereas the midportion of GS5-2 occupies the Phe-1 site, as evident from the distorted Phe304 and the I-helix (Figure 6B–D). The resulting hydrophobic, π–π, and cation–π interactions must be strong enough to keep GS5-2 bound during CYP3A4 crystallization.

dx.doi.org/10.1021/bi4005396 | *Biochemistry* 2013, 52, 4474–4481

CYP3A4–GS4 Complex. GS4 lacks both side groups (Figure 2) and, similar to GS5, has two binding sites in CYP3A4. Unlike GS5, both GS4 molecules, GS4-1 and GS4-2, are very well-defined in the crystal structure (Figure 6E,F). Heme-ligating GS4-1 is in an extended conformation and, similar to GS5-1, rotates by 180° (Figure 6G), whereas GS4-2 associates in a perpendicular mode. Having a more flexible and less branched backbone, GS4-2 closely approaches and curls around the midportion of GS4-1, filling the Phe-2 and Phe-1 sites with the head and end groups, respectively, and forming H-bonds with GS4-1 and the Phe108 and Arg372 main chain atoms (Figure 6F–H). Another distinguishing feature is the perpendicular orientation of the GS4-1 and GS4-2 thiazoles (Figure 6G), which promotes S–π rather than π–π stacking interactions observed for other ligands. GS4-2 imposes no steric hindrance on the 369–371 peptide but displaces the I-helix to the same extent as GS3. IPT of GS4-1 establishes multiple hydrophobic contacts with the surrounding residues but is partially solvent exposed (Figure 6H and Supporting Information Figure 4S). Again, to optimize interactions with this end group, the F–F′ loop adopts a novel conformation (Figure 6F and Supporting Information Figure 5S).

DISCUSSION

This study is an extension of our previous work on the interaction of human CYP3A4 with ritonavir-like compounds showing that (i) a strong and irreversible binding through the heme-ligating moiety is a prerequisite for potent CYP3A4 inhibition; (ii) the pyridine headgroup establishes a stronger Fe–N bond than the thiazole moiety; (iii) the desoxyritonavir backbone is more flexible and can adopt a conformation optimizing protein–ligand contacts; and (iv) the ligand binding mode may be influenced by nonbonding interactions provided by the side groups.[5−7] In this study, we tested in more detail the relative importance of the side and tail groups by comparing affinities, binding kinetics, and the association mode of five desoxyritonavir analogues (Figure 2). Here is an outline of our main findings.

First, our data indicate that the bulky hydrophobic side groups complicate heme binding kinetics and that the side group elimination or replacement with smaller moieties not only drastically lowers binding affinity and inhibitory potency for CYP3A4 but also leads to multiple ligand binding modes (Figure 3). The complex character of the heme ligation reaction is observed not only for the desoxyritonavir analogues. Association of CYP3A4 with ritonavir and a type I ligand bromoergoctiptine is also biphasic and has atypical k_{fast} on [ligand] dependence.[6,10] The biphasicity of the heme binding reaction may arise from the structural complexity and multiple conformations of these elongated substrates/inhibitors that enable molecules to enter the active site with either head or tail part first, and the conformational heterogeneity of CYP3A4 itself. The ligand chemical structure appears to define the k_{fast} on [ligand] dependence as well. The association rate of an ergot alkaloid bromoergoctiptine, one of the largest and highly hydrophobic CYP3A4 substrates, remains constant at low ligand concentrations and slightly increases (by ∼10%) when the ligand/protein ratio exceeds unity.[10] The k_{fast} vs [ritonavir] plot, on the other hand, is V-shaped, with a minimum at a ligand/protein ratio of ∼1,[6] which is very similar to the corresponding dependencies derived for GS6-GS8 (Figure 3M–O). As suggested previously, such deviation from hyperbolic kinetics could be caused by a rate-limiting process preceding heme ligation, e.g. ligand docking to a peripheral site prior to translocation to the active site cavity.[6,10] One such site is above the phenylalanine cluster, a unique feature of CYP3A4, to which progesterone is bound in the crystal structure.[11] Variations in the ligand size, hydrophobicity, backbone flexibility, and, according to this study, the side group structure could affect the manner of association with the peripheral site and, consequently, perturb the heme binding kinetics.

Second, comparison of the CYP3A4-inhibitor structures reveals a trend in the ligand binding process. Regardless of the side group chemical nature and the number of molecules bound, the space adjacent to the 369–371 peptide and Arg105 (Phe-2 site) is always occupied with no steric hindrance imposed (Figures 5 and 6). Such preferential occupancy suggests that this interaction site is critically important for tight binding. When possible, the ligands also try to fill the pocket adjacent to the I-helix (Phe-1 site), even if it leads to the I-helix displacement. The benefit of the resulting hydrophobic interactions overweighs the penalty for a conformational restraint. Clearly, one way for further ligand optimization could be Phe-1 substitution with a more flexible or smaller hydrophobic ring (i.e., hexane or pentane) placed at the same or next carbon atom.

Third, the side group size reduction increases ligand motional freedom within the active site, allowing the protein to mold the inhibitors in different ways to optimize contacts and fill the voids, which, in some cases, may require binding of more than one molecule. Multiple ligand binding to CYP3A4 is a well-known phenomenon confirmed by various techniques (reviewed in ref [12]). However, until now, the only direct evidence was the X-ray structure of the CYP3A4–ketoconazole complex, where two rigid drug molecules were bound in a closely associated, parallel mode.[13] The GS4/GS5–CYP3A4 models provide another glimpse on how multiple ligands can be arranged within the active site. Despite the contrasting ligand binding modes, perpendicular for GS4-1/GS4-2 and parallel for GS5-1/GS5-2 (Figure 6), there is virtually no difference in the overall CYP3A4 fold. Structural variations between the GS4-, GS5-, and other ligand-bound forms are observed only in the F–F′- and C-terminal loops, lining the top wall of the substrate binding pocket (Supporting Information Figure 5S). Thus, structural heterogeneity of the catalytic domain of CYP3A4 seems to arise exclusively from the conformational flexibility of these two surface elements.

Fourth, although Ser119 is hydrogen bonded only to GS6, our experimental results show that this residue markedly affects the affinity and binding kinetics of all studied compounds, especially GS4 and GS5 (Tables 1 and 2). Judging from the spectral perturbations (Figure 4), the latter ligands bind to the S119A variant only at one site and with a 7–12-fold lower affinity compared to WT. Also, the S119A mutation drastically slows down the GS7 and GS8 association (10–20-fold decrease in k_{fast}) and decreases T_m for all ligand-bound forms. We conclude, therefore, that the Ser119-mediated polar interactions are important for the CYP3A4-ligand association irrespective of whether the hydrogen bond with the ligand is formed or not.

Finally, on the basis of our data we conclude that IPT contributes to the ligand association process to a lesser extent and mainly through contacts with the F–F′-loop. Depending on orientation, IPT can establish polar, hydrophobic, π–π, and/or S–π interactions, through which the inhibitor midportion conformation and the Fe–N bond strength could

be modulated (Figures 3E, 5, and 6). Thus, a polyfunctional group would be preferable at the terminal end. Owing to high flexibility and adaptability of the F−F′-loop, capable of modulating protein−ligand interactions, and the limited structure/function data available, it is not possible now to predict what end group would be optimal. To do so, a more accurate assessment of the functional role of the terminal moiety and the possibility for its optimization need to be conducted using a wider range of ritonavir analogues.

■ ASSOCIATED CONTENT

Supporting Information

Kinetic data on association of GS4-GS8 to CYP3A4 S119A, comparison of the ritonavir and GS7 binding modes, electron density maps rendered around GS8 at different sigma levels, molecular surfaces and the F−F′ loop folding in the GS4−GS8-bound CYP3A4, and the X-ray data collection and model refinement statistics. This material is available free of charge via the Internet at http://pubs.acs.org.

Accession Codes

PDB ID codes: 4K9T, 4K9U, 4K9V, 4K9W, and 4K9X.

■ AUTHOR INFORMATION

Corresponding Author

*Tel: 1 949 8241953, Fax: 1 949 8243280, E-mail: sevrioui@uci.edu.

Funding

This work was supported by National Institutes of Health Grant GM33688, Gilead Sciences, Inc., and the California Center for Antiviral Drug Discovery

Notes

The authors declare no competing financial interest.

■ ACKNOWLEDGMENTS

This work involves research carried out at the Advanced Light Source and the Stanford Synchrotron Radiation Lightsource, a national user facility operated by Stanford University on behalf of the U.S. Department of Energy, Office of Basic Energy Sciences. The Advanced Light Source is supported by the Director, Office of Science, Office of Basic Energy Sciences, of the U.S. Department of Energy under Contract No. DE-AC02-05CH11231. The SSRL Structural Molecular Biology Program is supported by the Department of Energy, Office of Biological and Environmental Research, and by the National Institutes of Health, National Center for Research Resources, Biomedical Technology Program, and the National Institute of General Medical Sciences. We thank Lianhong Xu and Hong Ye of Gilead Sciences for synthesizing and providing the compounds used in this study.

■ ABBREVIATIONS

CYP3A4, 3A4 isoform of cytochrome P450; DMSO, dimethyl sulfoxide; DTMCR, desthiazolylmethyloxycarbonyl ritonavir; IPT, isopropyl thiazole; WT, wild type

■ REFERENCES

(1) Kempf, D. J., Marsh, K. C., Denissen, J. F., McDonald, E., Vasavanonda, S., Flentge, C. A., Green, B. E., Fino, L., Park, C. H., Kong, X. P., et al. (1995) ABT-538 is a potent inhibitor of human immunodeficiency virus protease and has high oral bioavailability in humans. *Proc. Natl. Acad. Sci. U. S. A. 92*, 2484−2488.

(2) Kempf, D. J., Marsh, K. C., Kumar, G., Rodrigues, A. D., Denissen, J. F., McDonald, E., Kukulka, M. J., Hsu, A., Granneman, G. R., Baroldi, P. A., Sun, E., Pizzuti, D., Plattner, J. J., Norbeck, D. W., and Leonard, J. M. (1997) Pharmacokinetic enhancement of inhibitors of the human immunodeficiency virus protease by coadministration with ritonavir. *Antimicrob. Agents Chemother. 41*, 654−660.

(3) Mathias, A. A., German, P., Murray, B. P., Wei, L., Jain, A., West, S., Warren, D., Hui, J., and Kearney, B. P. (2010) Pharmacokinetics and pharmacodynamics of GS-9350: a novel pharmacokinetic enhancer without anti-HIV activity. *Clin. Pharmacol. Ther. 87*, 322−329.

(4) Xu, L., Liu, H., Murray, B., Callebaut, C., Lee, M. S., Hong, A., Strickley, R. G., Tsai, L., K., Stray, K. M., Wang, Y., Rhodes, G. R., and Desai, M. C. (2010) Cobicistat (GS-9350): A potent and selective inhibitor of human CYP3A as a novel pharmacoenhancer. *ACS Med. Chem. Lett. 1*, 209−213.

(5) Sevrioukova, I. F., and Poulos, T. L. (2010) Structure and mechanism of the complex between cytochrome P4503A4 and ritonavir. *Proc. Natl. Acad. Sci. U. S. A. 107*, 18422−18427.

(6) Sevrioukova, I. F., and Poulos, T. L. (2012) Interaction of human cytochrome P4503A4 with ritonavir analogs. *Arch. Biochem. Biophys. 520*, 108−116.

(7) Sevrioukova, I. F., and Poulos, T. L. (2013) Pyridine-substituted desoxyritonavir is a more potent cytochrome P450 3A4 inhibitor than ritonavir. *J. Med. Chem. 56*, 3733−3741.

(8) CCP4. Collaborative computational project number 4. The CCP4 suite programs for protein crystallography. *Acta Crystallogr., Sect. D* 1994, *50*, 760−763.

(9) Emsley, P., Lohkamp, B., Scott, W. G., and Cowtan, K. (2010) Features and development of Coot. *Acta Crystallogr., Sect. D 66*, 486−501.

(10) Sevrioukova, I. F., and Poulos, T. L. (2012) Structural and mechanistic insights into the interaction of cytochrome P4503A4 with bromoergocryptine, a type I ligand. *J. Biol. Chem. 287*, 3510−3517.

(11) Williams, P. A., Cosme, J., Vinkovic, D. M., Ward, A., Angove, H. C., Day, P. J., Vonrhein, C., Tickle, I. J., and Jhoti, H. (2004) Crystal structures of human cytochrome P450 3A4 bound to metyrapone and progesterone. *Science 305*, 683−686.

(12) Sevrioukova, I. F., and Poulos, T. L. (2012) Understanding the mechanism of cytochrome P450 3A4: recent advances and remaining problems. *Dalton Trans. 42*, 3116−3126.

(13) Ekroos, M., and Sjogren, T. (2006) Structural basis for ligand promiscuity in cytochrome P450 3A4. *Proc. Natl. Acad. Sci. U. S. A. 103*, 13682−13687.